

Locally Conservative Discontinuous Petrov-Galerkin Finite Elements for Fluid Problems

Truman Ellis, Leszek Demkowicz, and Jesse Chan

Institute for Computational Engineering and Sciences,
The University of Texas at Austin,
Austin, TX 78712

Abstract

1 Introduction

The discontinuous Petrov-Galerkin (DPG) method with optimal test functions has been under active development for convection-diffusion type systems [5, 6, 10, 2, 11, 3, 14]. In this paper, we develop a theory for the locally conservative formulation of DPG for convection-diffusion type equations and supplement this with extensive numerical results.

1.1 Importance of Local Conservation

Locally conservative methods hold a special place for numerical analysts in the field of fluid dynamics. Perot[15] argues

Accuracy, stability, and consistency are the mathematical concepts that are typically used to analyze numerical methods for partial differential equations (PDEs). These important tools quantify how well the mathematics of a PDE is represented, but they fail to say anything about how well the physics of the system is represented by a particular numerical method. In practice, physical fidelity of a numerical solution can be just as important (perhaps even more important to a physicist) as these more traditional mathematical concepts. A numerical solution that violates the underlying physics (destroying mass or entropy, for example) is in many respects just as flawed as an unstable solution.

The discontinuous Petrov-Galerkin finite element method has been described as least squares finite elements with a twist. The key difference is that least square methods seek to minimize the residual of the solution in the L^2 norm, while DPG seeks the minimization in a dual norm realized through the inverse Riesz map. Exact mass conservation has been an issue that has plagued least squares finite elements for a long time. Several approaches have been used to try to adress this. Chang and Nelson[4] developed the *restricted LSFEM*[4] by augmenting the least squares equations with a Lagrange multiplier explicitly enforcing mass conservation element-wise. Our conservative formulation of DPG takes a similar approach and both methods share similar negative of transforming a minimization method to a saddle-point problem.

1.2 DPG is a Minimum Residual Method

Roberts *et al.* presents a brief history and derivation of DPG with optimal test functions in [16]. We follow his derivation of the standard DPG method as a minumum residual method. Let U be the trial Hilbert

space and V the test Hilbert space for a well-posed variational problem $b(u, v) = l(v)$. In operator form this is $Bu = l$, where $B : U \rightarrow V'$. We seek to minimize the residual for the discrete space $U_h \subset U$:

$$u_h = \arg \min_{u_h \in U_h} \frac{1}{2} \|Bu_h - l\|_{V'}^2. \quad (1)$$

Recalling that the Riesz operator $R_V : V \rightarrow V'$ is an isometry defined by

$$\langle R_V v, \delta v \rangle = (v, \delta v)_V, \quad \forall \delta v \in V,$$

we can use the Riesz inverse to minimize in the V -norm rather than its dual:

$$\frac{1}{2} \|Bu_h - l\|_{V'}^2 = \frac{1}{2} \|R_V^{-1}(Bu_h - l)\|_V^2 = \frac{1}{2} (R_V^{-1}(Bu_h - l), R_V^{-1}(Bu_h - l))_V. \quad (2)$$

The first order optimality condition for (2) requires the Gâteaux derivative to be zero in all directions $\delta u \in U_h$, i.e.,

$$(R_V^{-1}(Bu_h - l), R_V^{-1}B\delta u)_V = 0, \quad \forall \delta u \in U.$$

By definition of the Riesz operator, this is equivalent to

$$\langle Bu_h - l, R_V^{-1}B\delta u_h \rangle = 0 \quad \forall \delta u_h \in U_h. \quad (3)$$

Now, we can identify $v_{\delta u_h} := R_V^{-1}B\delta u_h$ as the optimal test function for trial function δu_h . Define $T := R_V^{-1}B : U_h \rightarrow V$ as the trial-to-test operator. Now we can rewrite (3) as

$$b(u_h, v_{\delta u_h}) = l(v_{\delta u_h}). \quad (4)$$

The DPG method then is to solve (4) with optimal test functions $v_{\delta u_h} \in V$ that solve the auxiliary problem

$$(v_{\delta u_h}, \delta v)_V = \langle R_V v_{\delta u_h}, \delta v \rangle = \langle B\delta u_h, \delta v \rangle = b(\delta u_h, \delta v), \quad \forall \delta v \in V. \quad (5)$$

Using a continuous test basis would result in a global solve for every optimal test function. Therefore DPG uses a discontinuous test basis which makes each solve element-local and much more computationally tractable. Of course, (5) still requires the inversion of the infinite-dimensional Riesz map, but approximating V by a finite dimensional V_h which is of a higher polynomial degree than U_h (hence “enriched space”) works well in practice.

No assumptions have been made so far on the definition of the inner product on V . In fact, proper choice of $(\cdot, \cdot)_V$ can make the difference between a solid DPG method and one that suffers from robustness issues.

2 Element Conservative Convection-Diffusion

We now proceed to develop a locally conservative formulation of DPG for convection-diffusion type problems, but there are a few terms that we need to define first. If Ω is our problem domain, then we can partition it into finite elements K such that

$$\bar{\Omega} = \bigcup_K \bar{K}, \quad K \text{ open},$$

with corresponding *skeleton* Γ_h and *interior skeleton* Γ_h^0 ,

$$\Gamma_h := \bigcup_K \partial K \quad \Gamma_h^0 := \Gamma_h - \Gamma.$$

We define broken Sobolev spaces element-wise:

$$H^1(\Omega_h) := \prod_K H^1(K),$$

$$\mathbf{H}(\text{div}, \Omega_h) := \prod_K \mathbf{H}(\text{div}, K).$$

We also need the trace spaces:

$$H^{\frac{1}{2}}(\Gamma_h) := \{\hat{v} = \{\hat{v}_K\} \in \prod_K H^{1/2}(\partial K) : \exists v \in H^1(\Omega) : v|_{\partial K} = \hat{v}_K\},$$

$$H^{-\frac{1}{2}}(\Gamma_h) := \{\hat{\sigma}_n = \{\hat{\sigma}_{Kn}\} \in \prod_K H^{-1/2}(\partial K) : \exists \boldsymbol{\sigma} \in \mathbf{H}(\text{div}, \Omega) : \hat{\sigma}_{Kn} = (\boldsymbol{\sigma} \cdot \mathbf{n})|_{\partial K}\},$$

which are developed more precisely in [16].

2.1 Derivation

Now that we have briefly outlined the abstract DPG method, let us apply it to the convection-diffusion equation. The strong form of the steady convection-diffusion problem with homogeneous Dirichlet boundary conditions reads

$$\begin{cases} \nabla \cdot (\boldsymbol{\beta}u) - \epsilon \Delta u = f & \text{in } \Omega \\ u = 0 & \text{on } \Gamma, \end{cases}$$

where u is the property of interest, $\boldsymbol{\beta}$ is the convection vector, and f is the source term. Nonhomogeneous Dirichlet and Neumann boundary conditions are straightforward but would add technicality to the following discussion. Let us write this as an equivalent system of first order equations:

$$\begin{aligned} \nabla \cdot (\boldsymbol{\beta}u - \boldsymbol{\sigma}) &= f \\ \frac{1}{\epsilon} \boldsymbol{\sigma} - \nabla u &= \mathbf{0}. \end{aligned}$$

If we then multiply the top equation by some scalar test function v and the bottom equation by some vector-valued test function $\boldsymbol{\tau}$, we can integrate by parts over each element K :

$$\begin{aligned} -(\boldsymbol{\beta}u - \boldsymbol{\sigma}, \nabla v)_K + ((\boldsymbol{\beta}u - \boldsymbol{\sigma}) \cdot \mathbf{n}, v)_{\partial K} &= (f, v)_K \\ \frac{1}{\epsilon} (\boldsymbol{\sigma}, \boldsymbol{\tau})_K + (u, \nabla \cdot \boldsymbol{\tau})_K - (u, \tau_n)_{\partial K} &= 0. \end{aligned} \tag{6}$$

The discontinuous Petrov-Galerkin method refers to the fact that we are using discontinuous optimal test functions that come from a space differing from the trial space. It does not specify our choice of trial space. Nevertheless, many considerations of DPG in the literature (convection-diffusion [7], linear elasticity [1], linear acoustics [9], Stokes [16]) associate DPG with the so-called “ultra-weak formulation.” We will follow the same derivation for the convection-diffusion equation, but we emphasize that other formulations are available. Thus, we seek field variables $u \in L^2(K)$ and $\boldsymbol{\sigma} \in \mathbf{L}^2(K)$. Mathematically, this leaves their traces on element boundaries undefined, and in a manner similar to the hybridized discontinuous Galerkin method, we define new unknowns for trace \hat{u} and flux \hat{t} . Applying these definitions to (6) and adding the two equations together, we arrive at our desired variational problem.

Find $\mathbf{u} := (u, \boldsymbol{\sigma}, \hat{u}, \hat{t}) \in \mathbf{U} := L^2(\Omega_h) \times \mathbf{L}^2(\Omega_h) \times H^{1/2}(\Gamma_h) \times H^{-1/2}(\Gamma_h)$ such that

$$\underbrace{-(\boldsymbol{\beta}u - \boldsymbol{\sigma}, \nabla v)_K + (\hat{t}, v)_{\partial K} + \frac{1}{\epsilon} (\boldsymbol{\sigma}, \boldsymbol{\tau})_K + (u, \nabla \cdot \boldsymbol{\tau})_K - (\hat{u}, \tau_n)_{\partial K}}_{b(\mathbf{u}, \mathbf{v})} = \underbrace{(f, v)_K}_{l(\mathbf{v})} \quad \text{in } \Omega \tag{7}$$

$$u = 0 \quad \text{on } \Gamma \tag{8}$$

$$(9)$$

for all $\mathbf{v} := (v, \boldsymbol{\tau}) \in \mathbf{V} := H^1(\Omega_h) \times \mathbf{H}(\text{div}, \Omega_h)$.

Let $\mathbf{U}_h := U_h \times \mathbf{S}_h \times \hat{U}_h \times \hat{F}_h \subset L^2(\Omega_h) \times \mathbf{L}^2(\Omega_h) \times H^{\frac{1}{2}}(\Gamma_h) \times H^{-\frac{1}{2}}(\Gamma_h)$ be a finite-dimensional subspace, and let $\mathbf{u}_h := (u_h, \boldsymbol{\sigma}_h, \hat{u}_h, \hat{t}_h) \in \mathbf{U}_h$ be a group variable. The element conservative DPG scheme is derived from the Lagrangian:

$$L(\mathbf{u}_h, \lambda_k) = \frac{1}{2} \|R_V^{-1}(b(\mathbf{u}_h, \cdot) - (f, \cdot))\|_{\mathbf{V}}^2 - \sum_K \lambda_K (b(\mathbf{u}_h, (1_K, \mathbf{0})) - l((1_K, \mathbf{0}))), \tag{10}$$

where $(1_K, \mathbf{0})$ is the test function in which $v = 1$ on element K and 0 elsewhere and $\boldsymbol{\tau} = \mathbf{0}$ everywhere.

Taking the Gâteaux derivatives as before, we arrive at the following system of equations:

$$\begin{cases} b(\mathbf{u}_h, T(\delta \mathbf{u}_h)) - \sum_K \lambda_K b(\mathbf{u}_h, (1_K, \mathbf{0})) = (f, T(\delta \mathbf{u}_h)) & \forall \delta \mathbf{u}_h \in \mathbf{U}_h \\ b(\mathbf{u}_h, (1_K, \mathbf{0})) = (f, (1_K, \mathbf{0})) & \forall K, \end{cases} \quad (11)$$

where $T := R_V^{-1} B : \mathbf{U}_h \rightarrow \mathbf{V}$ is the same trial-to-test operator as in the original formulation.

Since the trial-to-test operator selectively produces test functions in $H^1(\Omega_h)$ and $\mathbf{H}(\text{div}, \Omega_h)$, denote the result $v_{\delta \mathbf{u}_h}$ when $T(\delta \mathbf{u}_h) \in H^1(\Omega_h)$ and $\boldsymbol{\tau}_{\delta \mathbf{u}_h}$ when $T(\delta \mathbf{u}_h) \in \mathbf{H}(\text{div}, \Omega_h)$. Then, putting (11) into more concrete terms for convection-diffusion, we get:

$$\begin{cases} -(\beta u - \boldsymbol{\sigma}, \nabla v_{\delta \mathbf{u}_h}) + \langle \hat{t}, v_{\delta \mathbf{u}_h} \rangle + \frac{1}{\epsilon} (\boldsymbol{\sigma}, \boldsymbol{\tau}_{\delta \mathbf{u}_h}) + (u, \nabla \cdot \boldsymbol{\tau}_{\delta \mathbf{u}_h}) - \langle \hat{u}, \boldsymbol{\tau}_{\delta \mathbf{u}_h} \cdot \mathbf{n} \rangle \\ \quad - \sum_K \lambda_K (\delta \hat{t}, (1_K, \mathbf{0})) = (f, v_{\delta \mathbf{u}_h}) & \forall \delta \mathbf{u}_h \in \mathbf{U}_h \\ \langle \hat{t}, (1_K, \mathbf{0}) \rangle = (f, (1_K, \mathbf{0})) & \forall K. \end{cases} \quad (12)$$

2.2 Proof of Convergence

We cannot directly use Brezzi's theorem, but we can reproduce his argument. First of all, variational formulation (7) is equivalent to:

Find $\mathbf{u} \in \mathbf{U}$ such that

$$b(\mathbf{u}, T(\delta \mathbf{u})) = (f, T(\delta \mathbf{u})) \quad \forall \mathbf{v} \in \mathbf{V}. \quad (13)$$

This is because the trial-to-test operator $T = R_V^{-1} B$ is an isomorphism.

Restricting ourselves to $\delta \hat{t}_h \in \hat{F}_h^c$, and subtracting (13) from (12), we have the Galerkin orthogonality condition:

$$\begin{aligned} & \frac{1}{\epsilon} (\boldsymbol{\sigma}_h - \boldsymbol{\sigma}, \boldsymbol{\tau}_{\delta \mathbf{u}_h}) + (u_h - u, \nabla \cdot \boldsymbol{\tau}_{\delta \mathbf{u}_h}) - \langle \hat{u}_h - \hat{u}, \boldsymbol{\tau}_{\delta \mathbf{u}_h} \cdot \mathbf{n} \rangle \\ & - (\beta(u_h - u) - (\boldsymbol{\sigma}_h - \boldsymbol{\sigma}), \nabla v_{\delta \mathbf{u}_h}) + \langle \hat{t}_h - \hat{t}, v_{\delta \mathbf{u}_h} \rangle \\ & \quad \forall (\delta u_h, \delta \boldsymbol{\sigma}_h, \delta \hat{u}_h, \delta \hat{t}_h) \in U_h \times \mathbf{S}_h \times \hat{U}_h \times \hat{F}_h^c. \end{aligned} \quad (14)$$

We begin with an equivalent of Brezzi's *discrete inf-sup in kernel condition*.

Lemma 1. *The following condition holds:*

$$\begin{aligned} & \sup_{\substack{(\delta u_h, \delta \boldsymbol{\sigma}_h, \delta \hat{u}_h, \delta \hat{t}_h) \in \\ U_h \times \mathbf{S}_h \times \hat{U}_h \times \hat{F}_h^c}} \frac{|b((u_h, \boldsymbol{\sigma}_h, \hat{u}_h, \hat{t}_h), (v_{\delta \mathbf{u}_h}, \boldsymbol{\tau}_{\delta \mathbf{u}_h}))|}{\|(v_{\delta \mathbf{u}_h}, \boldsymbol{\tau}_{\delta \mathbf{u}_h})\|} \geq \alpha \|(u_h, \boldsymbol{\sigma}_h, \hat{u}_h, \hat{t}_h)\| \\ & \quad \forall (u_h, \boldsymbol{\sigma}_h, \hat{u}_h, \hat{t}_h) \in U_h \times \mathbf{S}_h \times \hat{U}_h \times \hat{F}_h^c. \end{aligned} \quad (15)$$

Proof. By the very construction of the trial-to-test operator, the supremum on the left is equal to

$$\|T(u_h, \boldsymbol{\sigma}_h, \hat{u}_h, \hat{t}_h)\|_V = \|R_V^{-1} B(u_h, \boldsymbol{\sigma}_h, \hat{u}_h, \hat{t}_h)\|_V = \|B(u_h, \boldsymbol{\sigma}_h, \hat{u}_h, \hat{t}_h)\|_V, \quad (16)$$

The condition follows now from the fact that operator B is bounded below, i.e. bilinear form $b((u_h, \boldsymbol{\sigma}_h, \hat{u}_h, \hat{t}_h), (v, \boldsymbol{\tau}))$ satisfies the inf-sup condition. \square

Assume additionally that flux decomposition (23) is orthogonal. We begin by decomposing \hat{t}_h ,

$$\hat{t}_h = \hat{t}_h^c + \hat{t}_h^{nc}. \quad (17)$$

Next, we use the triangle inequality,

$$\begin{aligned} \|(u - u_h, \boldsymbol{\sigma} - \boldsymbol{\sigma}_h, \hat{u} - \hat{u}_h, \hat{t} - \hat{t}_h)\| &= \|(u - u_h, \boldsymbol{\sigma} - \boldsymbol{\sigma}_h, \hat{u} - \hat{u}_h, \hat{t} - (\hat{t}_h^c + \hat{t}_h^{nc}))\| \\ &\leq \|(u - w_h, \boldsymbol{\sigma} - \boldsymbol{s}_h, \hat{u} - \hat{w}_h, \hat{t} - (\hat{r}_h^c + \hat{t}_h^{nc}))\| \\ &\quad + \|(w_h - u_h, \boldsymbol{s}_h - \boldsymbol{\sigma}_h, \hat{w}_h - \hat{u}_h, \hat{r}_h^c - \hat{t}_h^c)\| \end{aligned} \quad (18)$$

where $w_h \in U_h$, $\boldsymbol{s}_h \in \boldsymbol{S}_h$, $\hat{w}_h \in \hat{U}_h$, and $\hat{r}_h^c \in \hat{F}_h$ are arbitrary. The inf-sup in kernel condition now implies:

$$\begin{aligned} &\|(w_h - u_h, \boldsymbol{s}_h - \boldsymbol{\sigma}_h, \hat{w}_h - \hat{u}_h, \hat{r}_h^c - \hat{t}_h^c)\| \\ &\leq \frac{1}{\alpha} \sup_{\substack{(\delta u_h, \delta \boldsymbol{\sigma}_h, \delta \hat{u}, \delta \hat{t}) \in \\ U_h \times \boldsymbol{S}_h \times \hat{U}_h \times \hat{F}_h^c}} \frac{|b((w_h - u_h, \boldsymbol{s}_h - \boldsymbol{\sigma}_h, \hat{w}_h - \hat{u}_h, \hat{r}_h^c - \hat{t}_h^c), (v_{\delta u_h}, \boldsymbol{\tau}_{\delta u_h}))|}{\|(v_{\delta u_h}, \boldsymbol{\tau}_{\delta u_h})\|} \\ &\leq \frac{1}{\alpha} \sup_{\substack{(\delta u_h, \delta \boldsymbol{\sigma}_h, \delta \hat{u}, \delta \hat{t}) \in \\ U_h \times \boldsymbol{S}_h \times \hat{U}_h \times \hat{F}_h^c}} \frac{|b((w_h - u_h, \boldsymbol{s}_h - \boldsymbol{\sigma}_h, \hat{w}_h - \hat{u}_h, \hat{r}_h^c + \hat{t}_h^{nc} - \hat{t}), (v_{\delta u_h}, \boldsymbol{\tau}_{\delta u_h}))|}{\|(v_{\delta u_h}, \boldsymbol{\tau}_{\delta u_h})\|} \\ &\leq \frac{1}{\alpha} \|(w_h - u_h, \boldsymbol{s}_h - \boldsymbol{\sigma}_h, \hat{w}_h - \hat{u}_h, \hat{t} - (\hat{r}_h^c + \hat{t}_h^{nc}))\| \end{aligned} \quad (19)$$

where the second step follows from the Galerkin orthogonality condition (14), and the last step is a consequence of the minimum energy extension norm for fluxes. Cobining with (18), we get the final stability result:

$$\|(u - u_h, \boldsymbol{\sigma} - \boldsymbol{\sigma}_h, \hat{u} - \hat{u}_h, \hat{t} - \hat{t}_h)\| \leq \left(1 + \frac{1}{\alpha}\right) \inf_{\substack{(w_h, \boldsymbol{s}_h, \hat{w}, \hat{r}_h^c) \in \\ U_h \times \boldsymbol{S}_h \times \hat{U}_h \times \hat{F}_h^c}} \|(u - w_h, \boldsymbol{\sigma} - \boldsymbol{s}_h, \hat{u} - \hat{w}, \hat{t} - (\hat{r}_h^c + \hat{t}_h^{nc}))\|. \quad (21)$$

2.3 Local Problem

The optimal test functions are determined by solving local problems determined by the choice of test norm. There are several options to consider. The graph norm [8] is one of the most natural norms to consider as it is derived directly from the adjoint of the problem supplemented with (possibly scaled) L^2 field terms to upgrade it from a semi-norm. Chan *et al.* [3] derived a more robust alternative norm for convection diffusion (dubbed the robust norm). We recently developed a modification of the robust norm that appears to produce better results in the presence of singularities.

3 A coupled, robust test norm

In the course of our numerical experiments, we encountered unforeseen difficulties for certain problems under our current robust test norm. We illustrate in this section the observed issue using a second model problem with a singular solution, offer possible explanations for the phenomena observed, and propose a modification of the robust test norm presented previously, which we demonstrate eliminates the issues observed in numerical experiments.

3.1 A second model problem

We begin by first examining a different problem than convection-diffusion – we examine admissible solutions for the homogeneous Laplace's equation over the $y > 0$ half-plane under boundary conditions

$$\begin{aligned} u &= 0 \text{ on } x > 0 \\ \frac{\partial u}{\partial n} &= 0 \text{ on } x < 0. \end{aligned}$$

Let us consider the 2D case - a simple separation of variables argument in polar coordinates shows that the solution is of the form

$$u(r, \theta) = \sum_{n=0}^{\infty} R_n(r) \sin(\lambda_n \theta),$$

where $\lambda_n = n + \frac{1}{2}$, and $R_n(r) = C_{1,n}x^{\lambda_n} + C_{2,n}x^{-\lambda_n}$. By requiring $u(0, \theta) < \infty$, we have $R_n(r) = C_n x^{\lambda_n}$. We have now that solutions to this problem include u of the form

$$u = \sum_{n=0} x^{n+\frac{1}{2}} \sin \left(\left(n + \frac{1}{2} \right) \theta \right).$$

Note that even in the lowest-order term, the gradient of u displays a singularity at $r = 0$. **Find reference in that solutions to Laplace's equation always can be split into smooth and singular parts on similar domains.**

Consider now Laplace's equation $\Delta u = f$ on the box domain $\Omega = [0, 1]^2$ with boundary conditions

$$\begin{aligned} u &= 0 \text{ on } x > .5 \\ \frac{\partial u}{\partial n} &= 0 \text{ on } x < .5. \end{aligned}$$

with forcing term $f = 1$. Extrapolating the results from the half-plane example to a finite domain, we expect

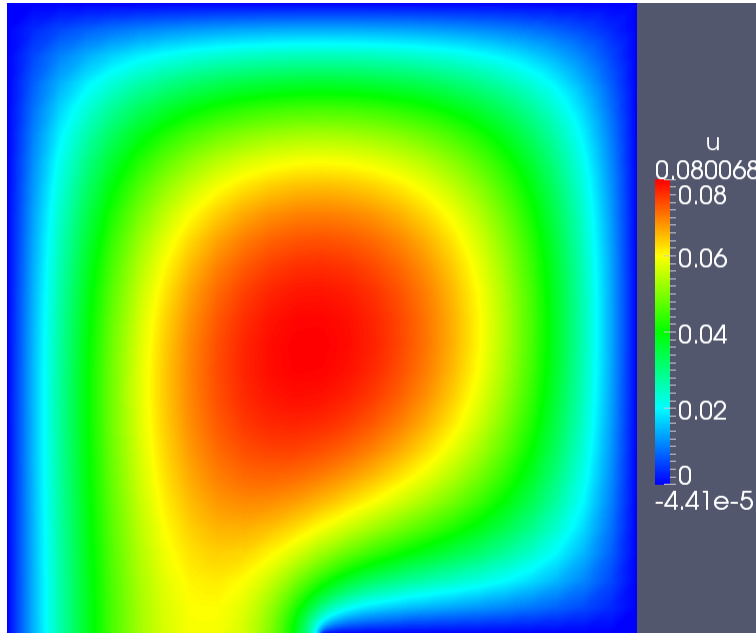


Figure 1: Solution of Laplace's equation on the unit quad with $f = 1$.

the solution of Laplace's equation to be bounded, but to have a singularity in its gradient. Figures 1 and 2 are finite element solutions of the above problem under a quadratic h -refined mesh. Figure 1 confirms that u is bounded, while Figure 2 confirms that singularities in the gradient appear at the point $(.5, 0)$, where the boundary condition changes from Neumann to Dirichlet.

We consider now the convection-diffusion problem, under a similar setup as before. We consider the domain $\Omega = [0, 1]^2$, with boundary conditions

$$\begin{aligned} u &= 0, & \text{on } x = 0 \\ \frac{\partial u}{\partial n} &= 0, & \text{on } x = 1, y = 1, \text{ and } y = 0, x < .5 \\ u &= 1, & \text{on } .5 < x \leq 1. \end{aligned}$$

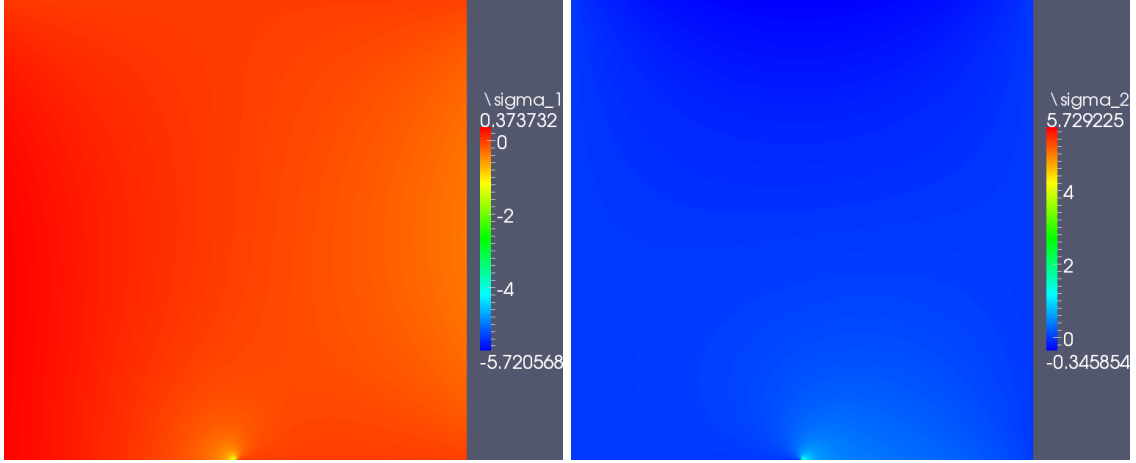


Figure 2: x and y components of the ∇u for u solving Laplace’s equation with a change in boundary conditions. Both components develop singularities at the point where the boundary condition changes type.

The problem is meant to simulate the transport of u over a domain with a “plate” boundary $x \in [.5, 1]$. For small ϵ , the problem develops a boundary layer over the plate, as well as a singularity at the plate tip $(x, y) = (.5, 0)$.¹ Unlike the Laplace example, we swap the Dirichlet boundary condition at the outflow $x = 1$ with an outflow boundary condition.²

The above convection-diffusion problem is related back to the earlier Laplace/diffusion problem with a singularity – in most of the domain, convective effects dominate; however, if we localize the behavior of Laplace’s equation to a circle of ϵ around $(.5, 0)$, then we again see a discontinuity in the stresses. Asymptotic expansion techniques indicate that singularities in solutions are determined primarily by the highest order differential operator present in the equation – in other words, the addition of a convective term to a scaled Laplacian (to recover the convection-diffusion equation) will not alter the presence of a singularity in the solution [17].

Figures 3 and 4 demonstrate the behavior of the DPG method under the robust test norm for the plate problem. The diffusion is taken to be fairly large ($\epsilon = 10^{-2}$), and automatic refinements are done until the element size h is at or below the diffusion scale. Due to the singular nature of the solution, refinements are clustered around $(.5, 0)$, and the order is set to be uniform with $p = 2$. While there should be no singularity in u , the magnitude of u grows as $h \rightarrow 0$, so long as $h \leq \epsilon$.

We note that the appearance of this non-physical singularity in u is allowed under the theory underlying the robust test norm; the error in the $L^2(\Omega)$ -norm of the solution is guaranteed to be robustly bounded; however, the $L^2(\Omega)$ norm does allow for the presence of weak singularities (singularities of order $x^{-\frac{1}{2}}$). Apart from the oscillation of u at the singular point, the solution is well-behaved, and the stress $\sigma = \epsilon \nabla u$ is very well represented, as indicated in Figure 5.

3.2 A modification of the robust test norm

While oscillations of this sort in a solution near a singular point may be acceptable in certain simulations, it is a large problem for the methods in compressible flow simulations – physical constraints require several solution variables to remain positive throughout simulation.³ We propose a modification of the robust test

¹This problem is meant to mimic the Carter flat plate problem – a common early benchmark problem in viscous compressible flow problems – which can be shown to also exhibit a singularity in stress at the point $(.5, 0)$.

²The outflow “boundary condition” is simply the absence of an applied boundary condition, and is analyzed in more detail in [13]. This outflow condition appears to work well for convection-diffusion problems in the convective regime, and is the outflow condition we will use in our extension of DPG to a model problem in viscous compressible flow. Though the well-posedness of the problem under this boundary condition is questionable, we can still effectively illustrate the issues present under the robust test norm using this problem setup.

³Apart from returning a non-physical solution, the violation of positivity constraints typically results in non-convergence of nonlinear solvers.

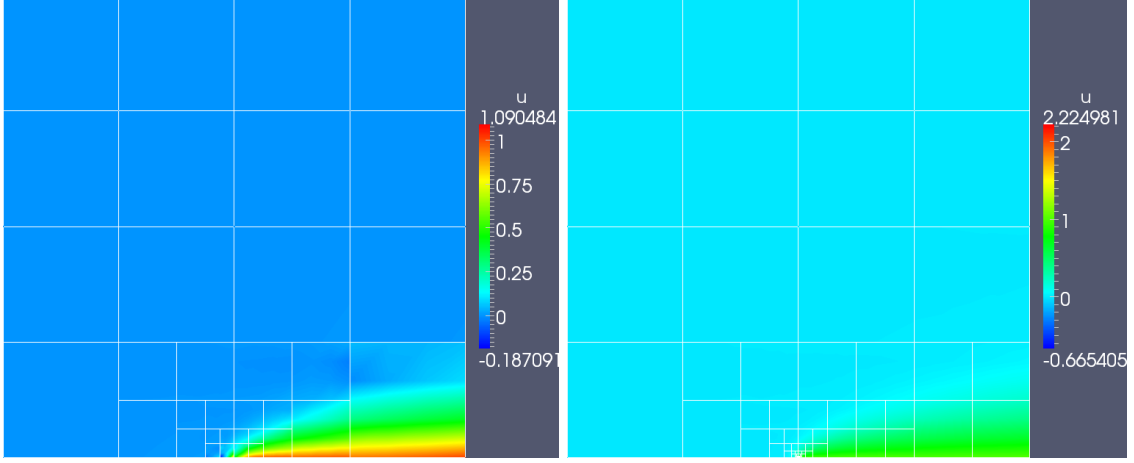


Figure 3: Solution u for $\epsilon = .01$ under the robust test norm. The solution oscillates strongly at the plate edge, growing in magnitude under additional refinements despite the absence of a singularity in u at that point.

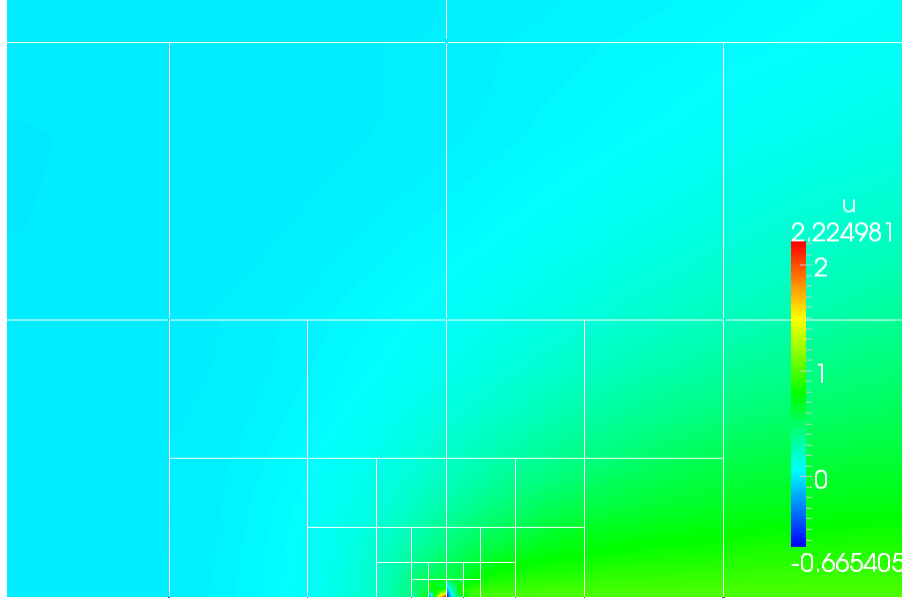


Figure 4: Zoomed solution u and adaptive mesh for $\epsilon = .01$ after over-resolution of the diffusion scale.

norm that appears to remedy this issue, which we refer to as

$$\|(v, \tau)\|_V^2 := \|v\|_{L^2(\Omega)}^2 + \|\beta \cdot \nabla v\|_{L^2(\Omega)}^2 + \|\nabla \cdot \tau - \beta \cdot \nabla v\|_{L^2(\Omega)}^2 + \|C_\tau \tau\|_{L^2(\Omega)}^2,$$

where C_τ is defined as before.⁴ We note that, under the theory developed in the above test norm is trivially provably robust using the same theory.⁵

While not rigorously understood, the author believes the issues related to the appearance of non-physical singularities to be related to the uncoupled nature of the test norm. Previous example problems exhibited boundary layers and sharp gradients in the stress σ , but not singularities, which contribute significantly

⁴We note that we have dropped the mesh-dependent scaling on $\|v\|_{L^2(\Omega)}$ from the robust norm; this is related to recent insights into the nature of DPG test spaces and explained in more detail in

⁵This is due to the fact that $\|\nabla \cdot \tau - \beta \cdot \nabla v\|_{L^2(\Omega)}^2$ is robustly bounded by $\|\nabla \cdot \tau\|_{L^2(\Omega)}$ and $\|\beta \cdot \nabla v\|_{L^2(\Omega)}$. Alternatively, we can note that $\|\nabla \cdot \tau - \beta \cdot \nabla v\|_{L^2(\Omega)}^2 = \|g\|_{L^2(\Omega)}^2$, where g is a load of the adjoint problem related to robustness described in

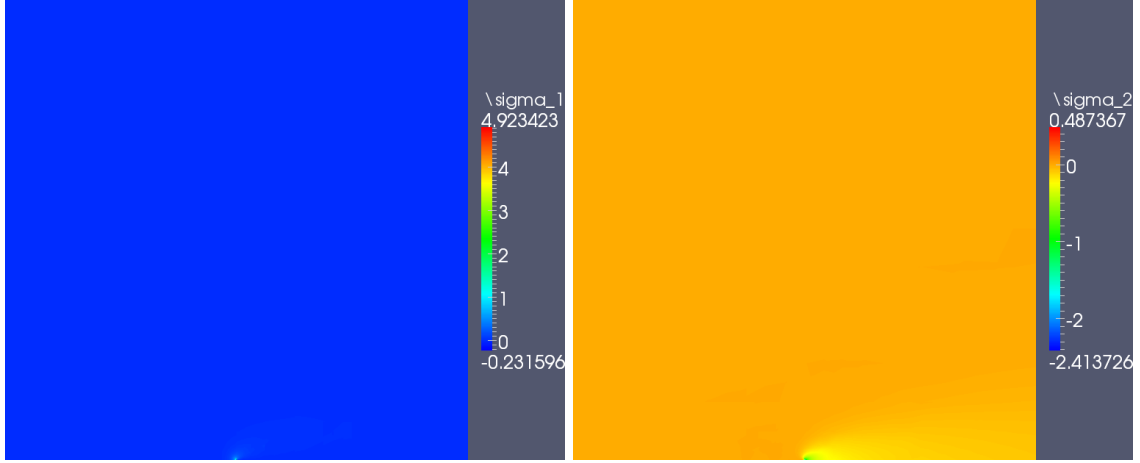


Figure 5: Viscous stresses for the plate problem.

more error. We expect that the oscillations observed in u are a sort of *pollution error*, where error in u is tied to error in σ . If we consider the ultra-weak variational formulation for convection-diffusion

$$(u, \nabla \cdot \tau - \beta \cdot \nabla v)_{L^2(\Omega)} + \left(\sigma, \frac{1}{\epsilon} \tau + \nabla v \right)_{L^2(\Omega)} + \dots,$$

we can see that it is a combination of test functions that corresponds to both u and σ . Recall from the previous section that, by choosing τ and v such that they satisfy the adjoint equation with forcing terms u and σ , we recover the best L^2 approximation. In other words, achieving optimality in the L^2 norm requires coupling between v and τ , which is achieved under the graph norm, but not the robust norm derived in the previous section. If coupling of the test terms, we expect that decoupling v and τ from each other in a test norm from each other will have the effect of coupling error in σ to error in u , which would explain the spurious oscillations in u in the presence of singularities in σ . Similar results have been observed in the Stokes equations, where error in u is coupled to the behavior of the pressure variable [12].

The drawback to using the above test norm is that the resulting local system for test functions is now completely coupled, whereas using the previous test norm, the system was block diagonal due to the decoupling in v and τ and could be constructed and inverted more efficiently. We hope to explore the difference between these two norms in more rigor and detail in the future.

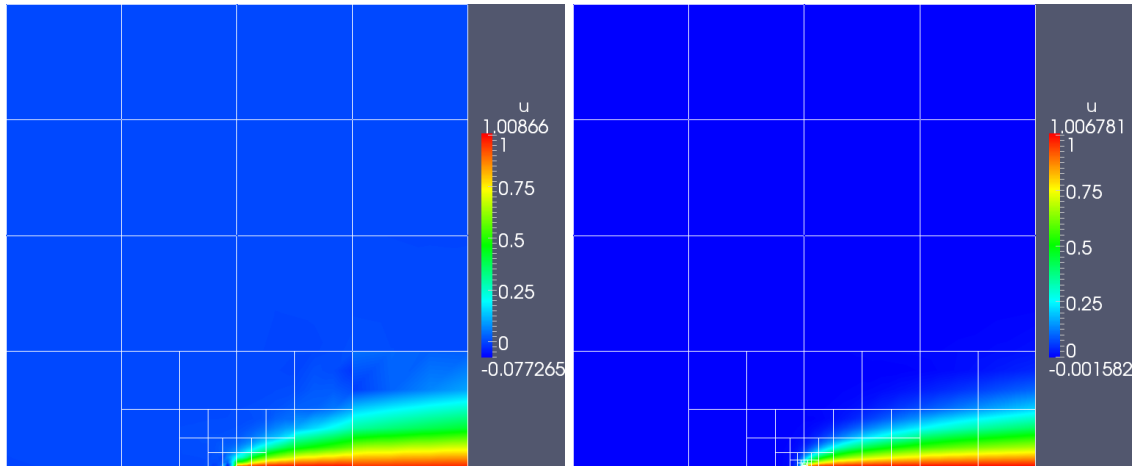


Figure 6: $\epsilon = 10^{-2}$ without h -resolving diffusion scale, and with h -resolution of diffusion scale.

Figure 6 shows the solution for $\epsilon = .01$, where the diffusion scale is both underresolved and resolved by

h -adaptivity. In both cases, there are no additional oscillations near the plate tip – Figure 7 shows a zoomed image of the solution u at the point $(.5, 0)$. The stress is resolved similarly to the previous case; however, the solution u does not display spurious oscillations in either the underresolved or resolved cases. Figure 8 displays the same quantities, but for $\epsilon = 10^{-4}$, in order to demonstrate that the new test norm removes spurious oscillations in u (in the presence of singularities in σ) independently of ϵ .

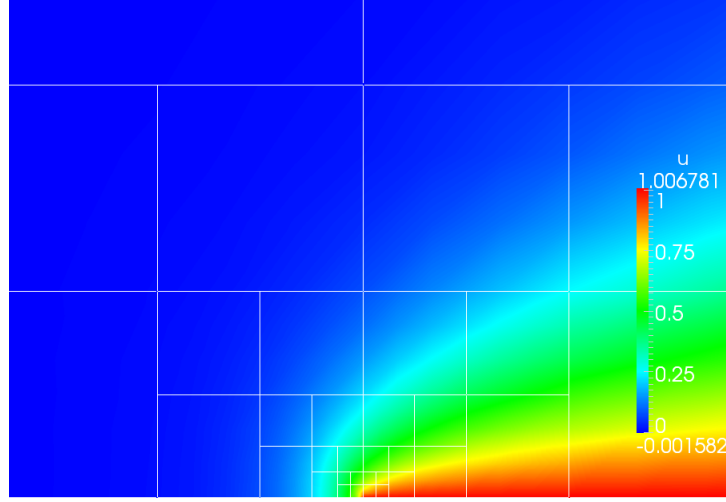


Figure 7: Zoom of solution u at the plate tip for $\epsilon = 10^{-2}$.

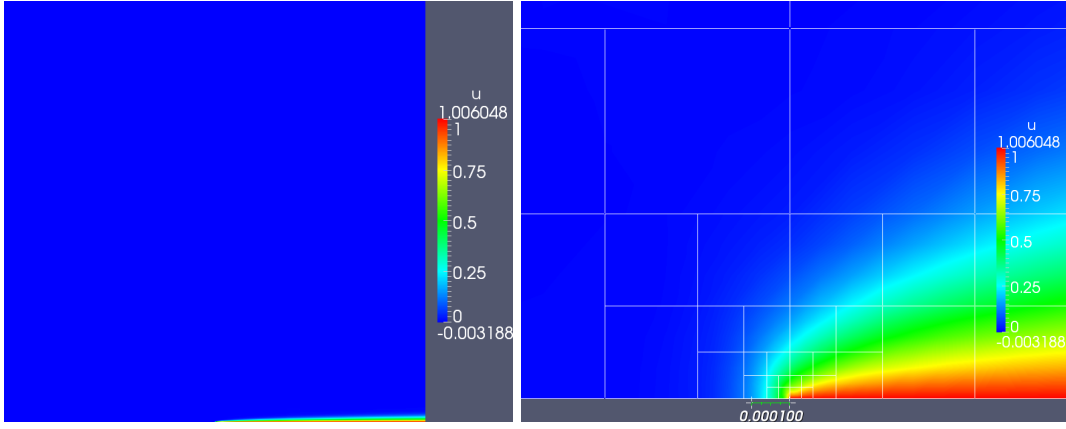


Figure 8: 14 refinements for $\epsilon = 10^{-4}$, $\min h$ is $O(10^{-5})$.

3.2.1 Robust Norm

For illustrative purposes we choose the robust test norm developed by Chan *et al.* [3]. With this choice, we get our local problem:

Find $v_{\delta \mathbf{u}_h} \in H^{-1}(K)$, $\boldsymbol{\tau}_{\delta \mathbf{u}_h} \in \mathbf{H}(\text{div}, K)$ such that:

$$\begin{aligned} (\nabla \cdot \boldsymbol{\tau}_{\delta \mathbf{u}_h}, \nabla \cdot \delta \boldsymbol{\tau})_K + \min \left\{ \frac{1}{\epsilon}, \frac{1}{|K|} \right\} (\boldsymbol{\tau}_{\delta \mathbf{u}_h}, \delta \boldsymbol{\tau})_K + \epsilon (\nabla v_{\delta \mathbf{u}_h}, \nabla \delta v)_K + (\boldsymbol{\beta} \cdot \nabla v_{\delta \mathbf{u}_h}, \boldsymbol{\beta} \cdot \nabla \delta v)_K \\ + \alpha \min \left\{ \sqrt{\frac{\epsilon}{|K|}}, 1 \right\} (v_{\delta \mathbf{u}_h}, \delta v)_K = b(\delta \mathbf{u}_h, (\delta v, \delta \boldsymbol{\tau})) \quad \forall \delta v \in H^{-1}(K), \delta \boldsymbol{\tau} \in \mathbf{H}(\text{div}, K), \end{aligned} \quad (22)$$

where, typically, $\alpha = 1$.

We can decompose the discrete flux space \hat{F}_h into element conserving fluxes and some algebraic complement:

$$\hat{F}_h = \hat{F}_h^c \oplus \hat{F}_h^{nc}, \quad \hat{F}_h^c := \{\hat{t} : \langle \hat{t}, (1_K, \mathbf{0}) \rangle = 0 \quad \forall K\}. \quad (23)$$

This may be accomplished by employing for fluxes in \hat{F}_h^c traces of curls, $\nabla \times \phi$.

In practice, we solve (12) as a fully coupled system of equations, but for didactic purposes, we can examine it one piece at a time. If we restrict (12)₁ to $\delta\hat{t} \in \hat{F}_h^{nc}$, the Lagrange multiplier term drops out and we left with a system that we can solve for u_h , σ_h , \hat{u}_h , and $\hat{t}_h^c \in \hat{F}_h^c$.

Restricting ourselves to $\delta\hat{t} \in \hat{F}_h^c$ in (12)₁, we obtain a system of equations that can be solved for u_h , σ_h , \hat{u}_h , and $\hat{t} \in \hat{F}_h^c$. The remaining fluxes, $\hat{t} \in \hat{F}_h^{nc}$ are determined from (12)₂. Finally, testing with $\hat{t} \in \hat{F}_h^{nc}$ in (12)₁, we obtain a system of equations that can be solved for Lagrange multipliers λ_K .

Additionally, we can pass in local problem (22) with $\alpha \rightarrow 0$. The fact that the test functions will be determined then up to a constant does not matter, for $\delta\hat{t} \in \hat{F}_h^c$, equation (12)₁ is orthogonal to constants. Mathematically, we are dealing with equivalence classes of functions, but in order to obtain a single function that we can deal with numerically, we replace the alpha term with a zero mean scaling condition to obtain the new test norm,

$$(\nabla \cdot \tau_{\delta u_h}, \nabla \cdot \delta \tau)_K + \min \left\{ \frac{1}{\epsilon}, \frac{1}{|K|} \right\} (\tau_{\delta u_h}, \delta \tau)_K + \epsilon (\nabla v_{\delta u_h}, \nabla \delta v)_K + (\beta \cdot \nabla v_{\delta u_h}, \beta \cdot \nabla \delta v)_K + \frac{1}{|K|^2} \int_K v_{\delta u_h} \delta v, \quad (24)$$

where the $\frac{1}{|K|^2}$ coefficient is needed to make the zero mean term scale correctly with h . Numerically this helps a good deal with the condition numbers of the local solve.

It is convenient to be able to take $\alpha \rightarrow 0$ as we will see in some later numerical experiments.

4 Numerical Experiments

In 4.1 we define each numerical experiment, and in 4.2 we discuss the solution properties in general. We solve with second order field variables and flux (u , σ , and \hat{t}), third order traces (\hat{t}), and fifth order test functions (v and τ).

Describe how we check local conservation.

4.1 Description of Problems

Unless otherwise noted, the problem domain is $\Omega = [0, 1]^2$ and $f = 0$. Also note that except for the discontinuous source problem, blue corresponds to $u = 0$ and red to $u = 1$ with a linear scaling in between.

4.1.1 Erickson-Johnson Model Problem

The Erickson-Johnson problem is one of the few convection-diffusion problems with a known analytical solution. Take $\beta = (1, 0)^T$ and boundary conditions $\hat{t} = \beta \cdot \mathbf{n}u_0$ when $\beta_n \leq 0$, where u_0 is the trace of the exact solution, and $\hat{u} = 0$ when $\beta_n > 0$. For $n = 1, 2, \dots$, let $\lambda_n = n^2 \pi^2 \epsilon$, $r_n = \frac{1 + \sqrt{1 + 4\epsilon \lambda_n}}{2\epsilon}$, and $s_n = \frac{1 - \sqrt{1 + 4\epsilon \lambda_n}}{2\epsilon}$. The exact solution is

$$u(x, y) = C_0 + \sum_{n=1}^{\infty} C_n \frac{\exp(s_n(x-1)) - \exp(r_n(x-1))}{r_n \exp(-s_n) - s_n \exp(-r_n)} \cos(n\pi y). \quad (25)$$

Taking $\epsilon = 10^{-2}$, $C_1 = 1$, and $C_{n \neq 1} = 0$, the exact solution looks like Figure 9.

4.1.2 Skewed Convection-Diffusion Problem

This is a standard convection-diffusion problem with a skewed convection vector relative to the mesh. We take $\beta = (2, 1)$, and on the left and bottom inflow boundaries we impose $\hat{t} = 1 - x - y$ while the right and top boundaries have $\hat{u} = 0$. We solve for $\epsilon = 10^{-4}$.

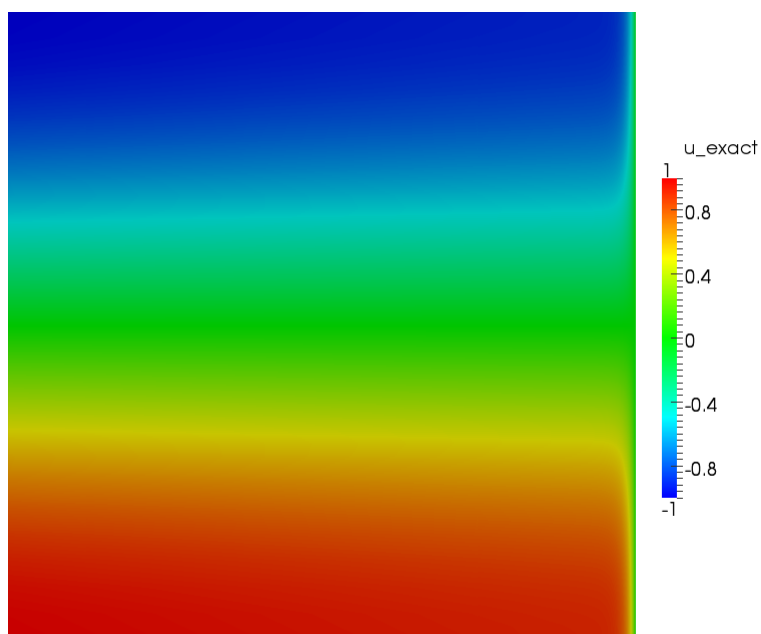


Figure 9: Erickson-Johnson exact solution

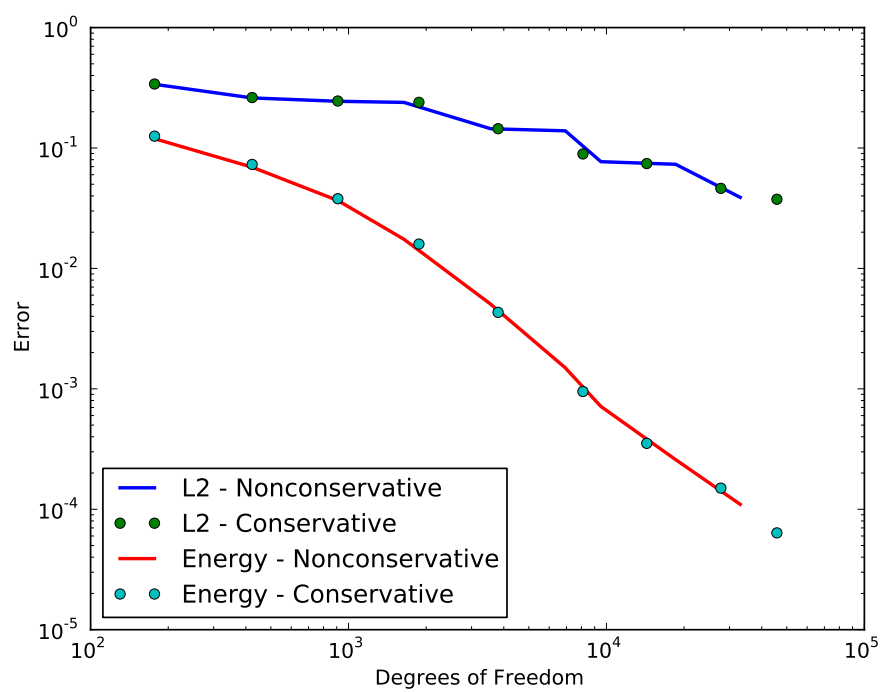


Figure 10: Error in Erickson-Johnson solutions

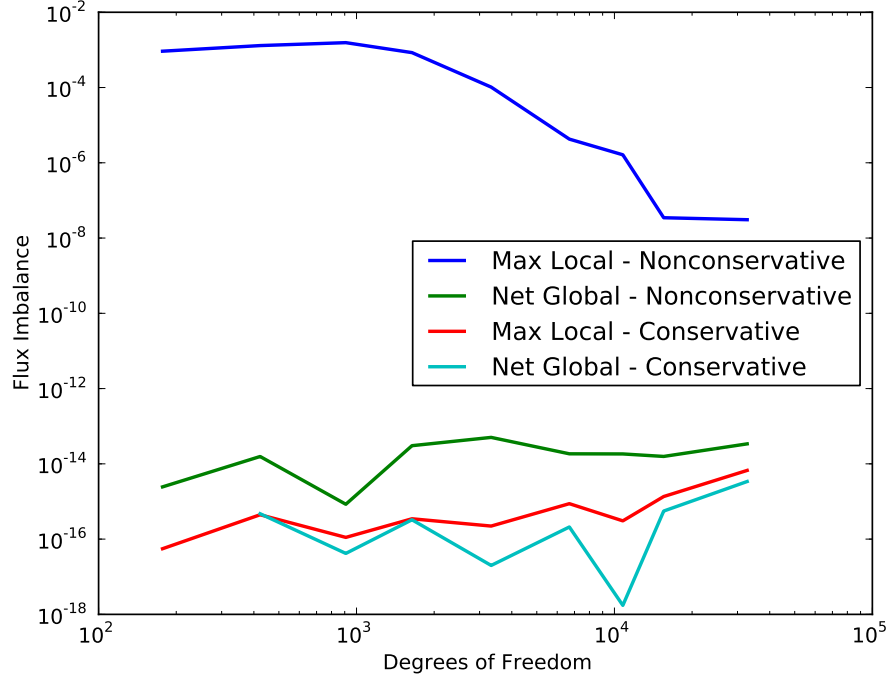


Figure 11: Flux imbalance in Erickson-Johnson solutions

4.1.3 Double Glazing Problem

This nominal problem definition takes the same unit square domain with

$$\boldsymbol{\beta} = \begin{pmatrix} 2(2y-1)(1-(2x-1)^2) \\ -2(2x-1)(1-(2y-1)^2) \end{pmatrix}; \quad \hat{u} = \begin{cases} 1 & \text{on } \Gamma_{right} \\ 0 & \text{else} \end{cases},$$

except that this definition for the boundary is not legal for $\hat{u} \in H^{\frac{1}{2}}(\Gamma_h)$ which is continuous. Therefore we use a ramp of width $\sqrt{\epsilon}$ on the right edge to go from 0 to 1. The results are for $\epsilon = 10^{-2}$.

4.1.4 Vortex Problem

This problem models a mildly diffusive vortex convecting fluid in a circle. We deal with domain $\Omega = [-1, 1]^2$, with $\epsilon = 10^{-4}$, and $\boldsymbol{\beta} = (-y, x)^T$. Note that $\boldsymbol{\beta} = \mathbf{0}$ at the domain center. We have an inflow boundary condition when $\boldsymbol{\beta} \cdot \mathbf{n} < 0$, in which case we set $\hat{t} = \boldsymbol{\beta} \cdot \mathbf{n} \cdot u_0$ where $u_0 = \frac{\sqrt{x^2+y^2}-1}{\sqrt{2}-1}$ which will vary from 0 at the center of boundary edges to 1 at corners. We don't enforce an outflow boundary.

4.1.5 Wedge Problem

We devised this problem to examine some of the issues we were having blow up of the solution under the robust test norm. The domain is a rectangle $[-0.5, 0.5] \times [-1, 0.5]$ where the triangle connecting the bottom edges with the origin at $(0, 0)$ is removed. The convection vector $\boldsymbol{\beta} = (1, 0)^T$, $\epsilon = 10^{-1}$, and we apply boundary conditions $\hat{t} = 0$ on the left inflow edge, $\hat{u} = 0$ on the top edge, $\boldsymbol{\beta} \cdot \mathbf{n} \cdot \hat{u} - \hat{t} = \sigma_n = 0$ on the right outflow edge, $\hat{u} = 1$ on the leading edge of the wedge, and $\hat{t} = \boldsymbol{\beta} \cdot \mathbf{n} \cdot 1$ on the trailing edge of the wedge.

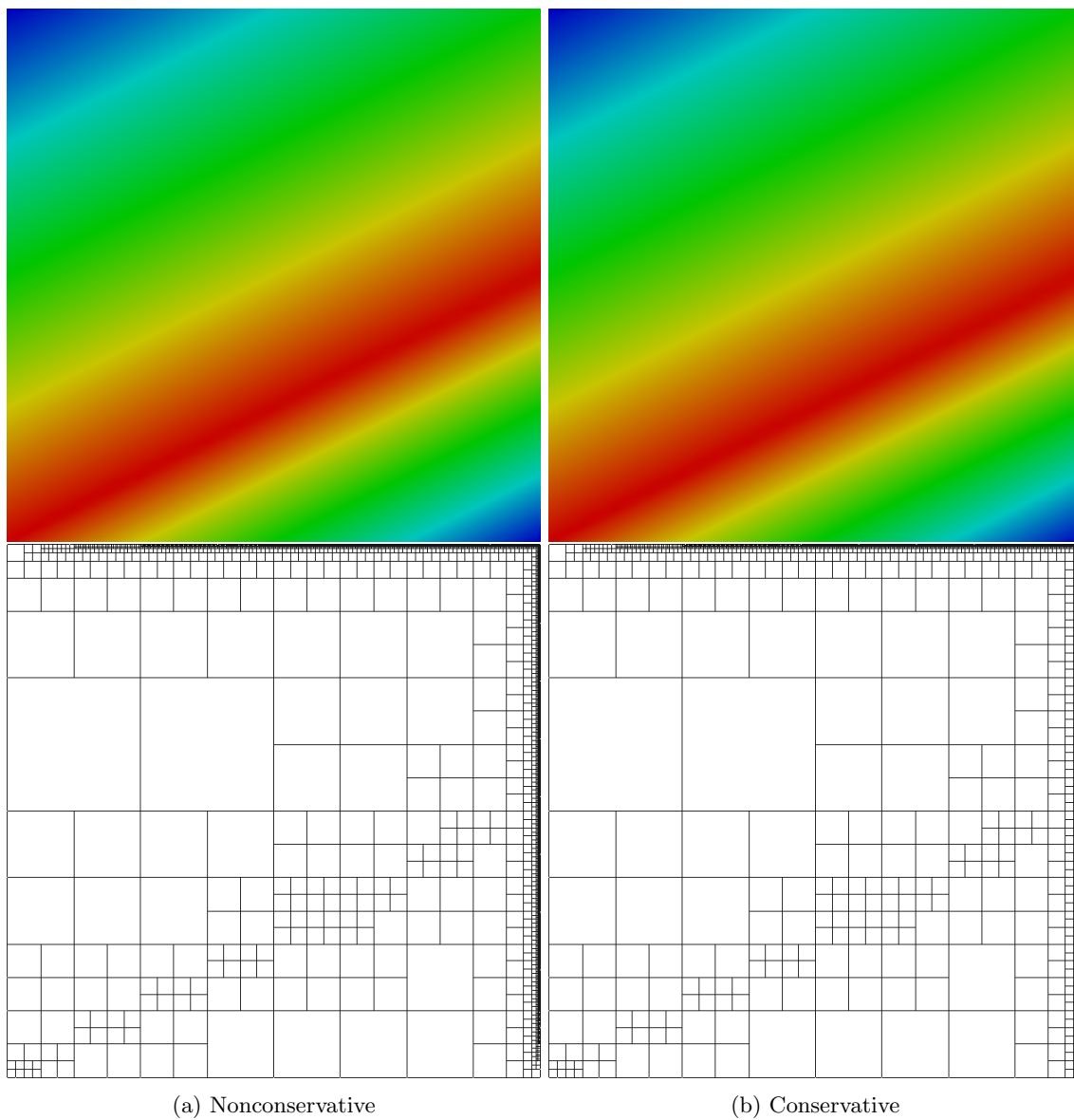


Figure 12: Skewed convection-diffusion problem after 8 refinements

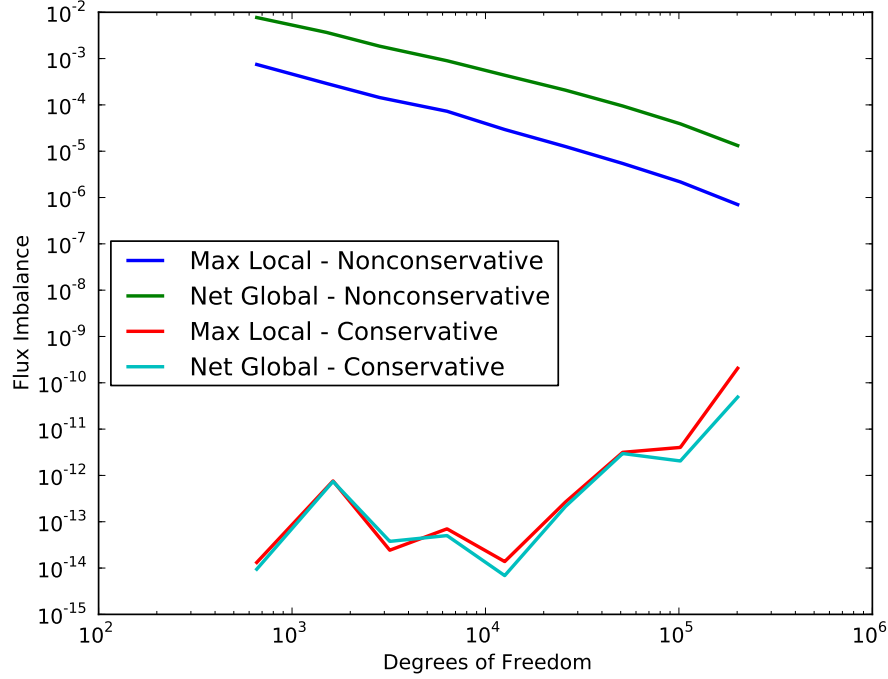


Figure 13: Flux imbalance in skewed convection-diffusion solutions

4.1.6 Inner Layer Problem

In this problem, $\beta = (\frac{\sqrt{3}}{2}, \frac{1}{2})^T$ and we have a discontinuous flux inflow condition where $\hat{t} = 0$ if $y \leq 0.2$ and $\hat{t} = \beta \cdot \mathbf{n}$ if $y > 0.2$. On the outflow, $\hat{u} = 0$. We use a very small diffusion scale of $\epsilon = 10^{-6}$ which creates a very thin inner layer.

4.1.7 Discontinuous Source Problem

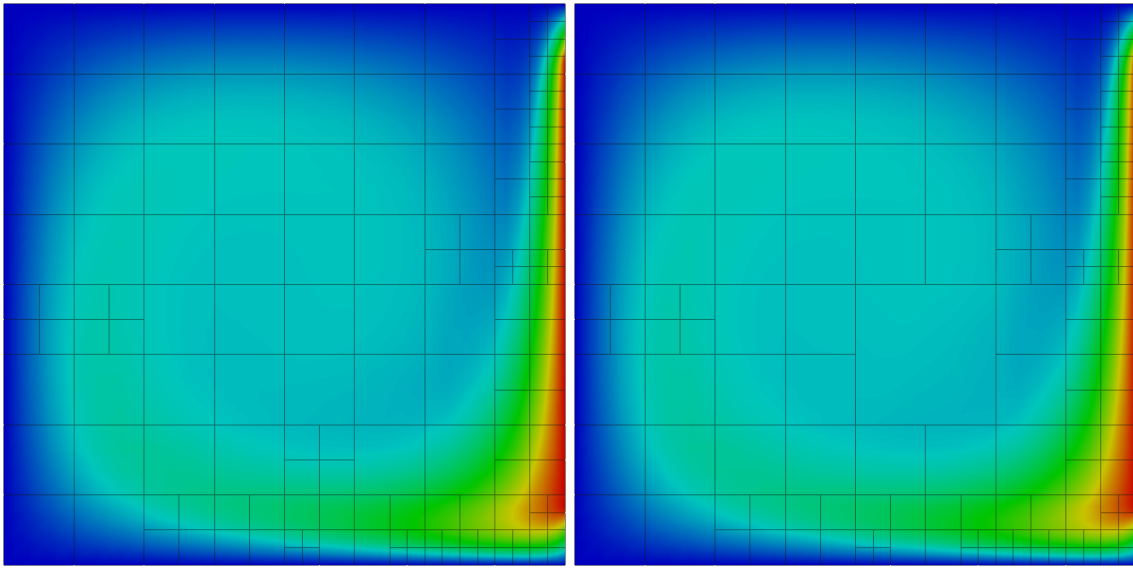
Here, $\beta = (0.5, 1)^T / \sqrt{1.25}$, and we have a discontinuous source term such that $f = 1$ when $y \geq 2x$ and $f = -1$ when $y < 2x$. We apply boundary conditions of $\hat{t} = 0$ on the inflow and $\hat{u} = 0$ on the outflow. Contrary to the other problems discussed, the solution for this problem does not range from 0 to one. Rather, the colorbar in Figure 22 is scaled to $[-1.110, 0.889]$.

4.1.8 Hemker Problem

The Hemker problem is defined on a domain $\Omega = \{[-3, 9] \times [-3, 3]\} \setminus \{(x, y) : x^2 + y^2 < 1\}$, essentially a simplified model of flow past an infinite cylinder. We start with the initial mesh shown in Figure 24 in which we approximate the circle by 8 fourth order curvilinear polynomial segments. As we refine, the new elements are fitted to better approximate an exact circle. The boundary conditions are $\hat{t} = \beta \cdot \mathbf{n} \cdot 1$ on the left inflow boundary, $\beta \cdot \mathbf{n} \cdot \hat{u} - \hat{t} = \sigma_n = 0$ on the right outflow boundary, $\hat{t} = 0$ on the top and bottom edges, and $\hat{u} = 1$ on the cylinder.

4.2 Analysis of Results

The general trend we see looking at the results is that the solution quality of the conservative and nonconservative formulations is nearly identical. This is ideal, as we wish to preserve the attractive features of DPG – namely that it minimizes error in the energy norm. In particular, when we examine the error convergence



(a) Nonconservative

(b) Conservative

Figure 14: Double glazing problem after 5 refinements

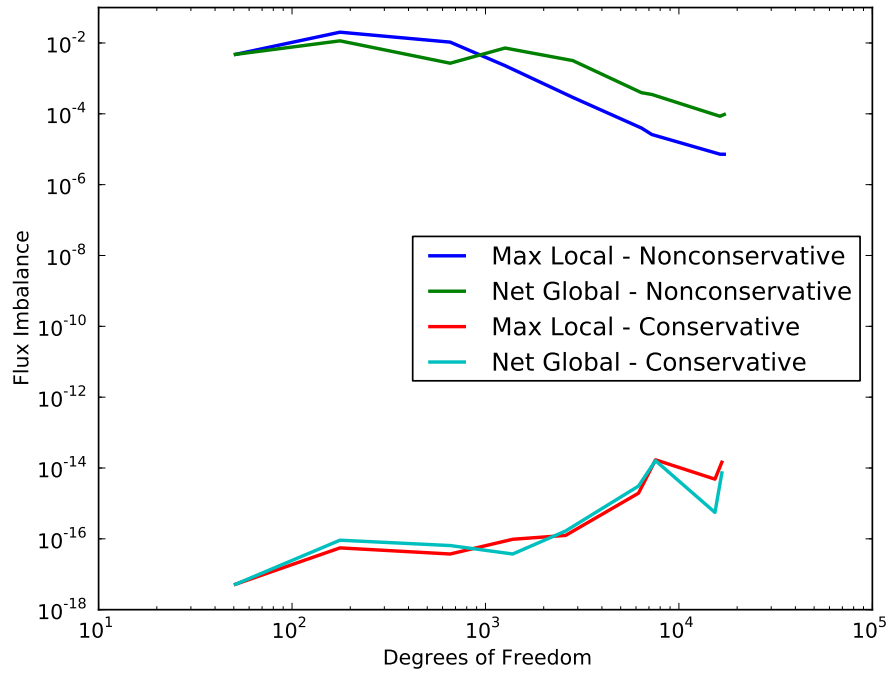
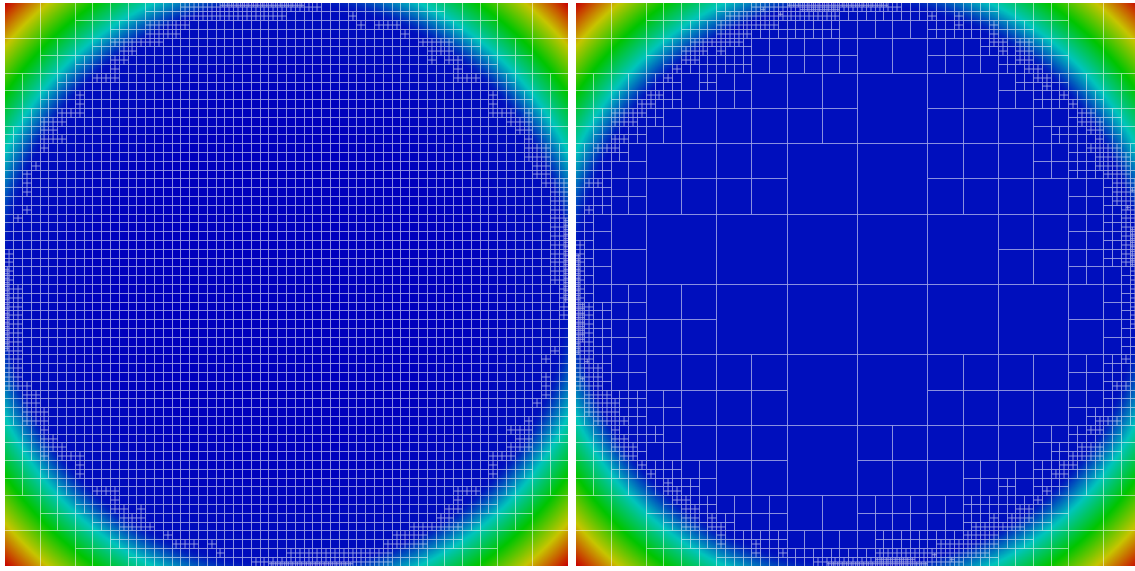


Figure 15: Flux imbalance in double glazing problem



(a) Nonconservative

(b) Conservative

Figure 16: Vortex problem after 6 refinements

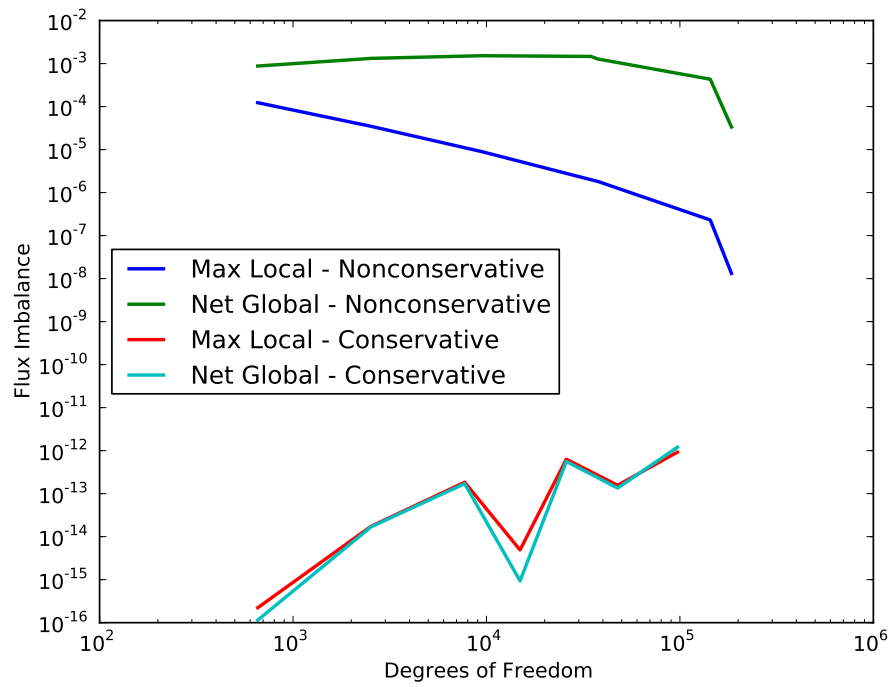


Figure 17: Flux imbalance in vortex solutions

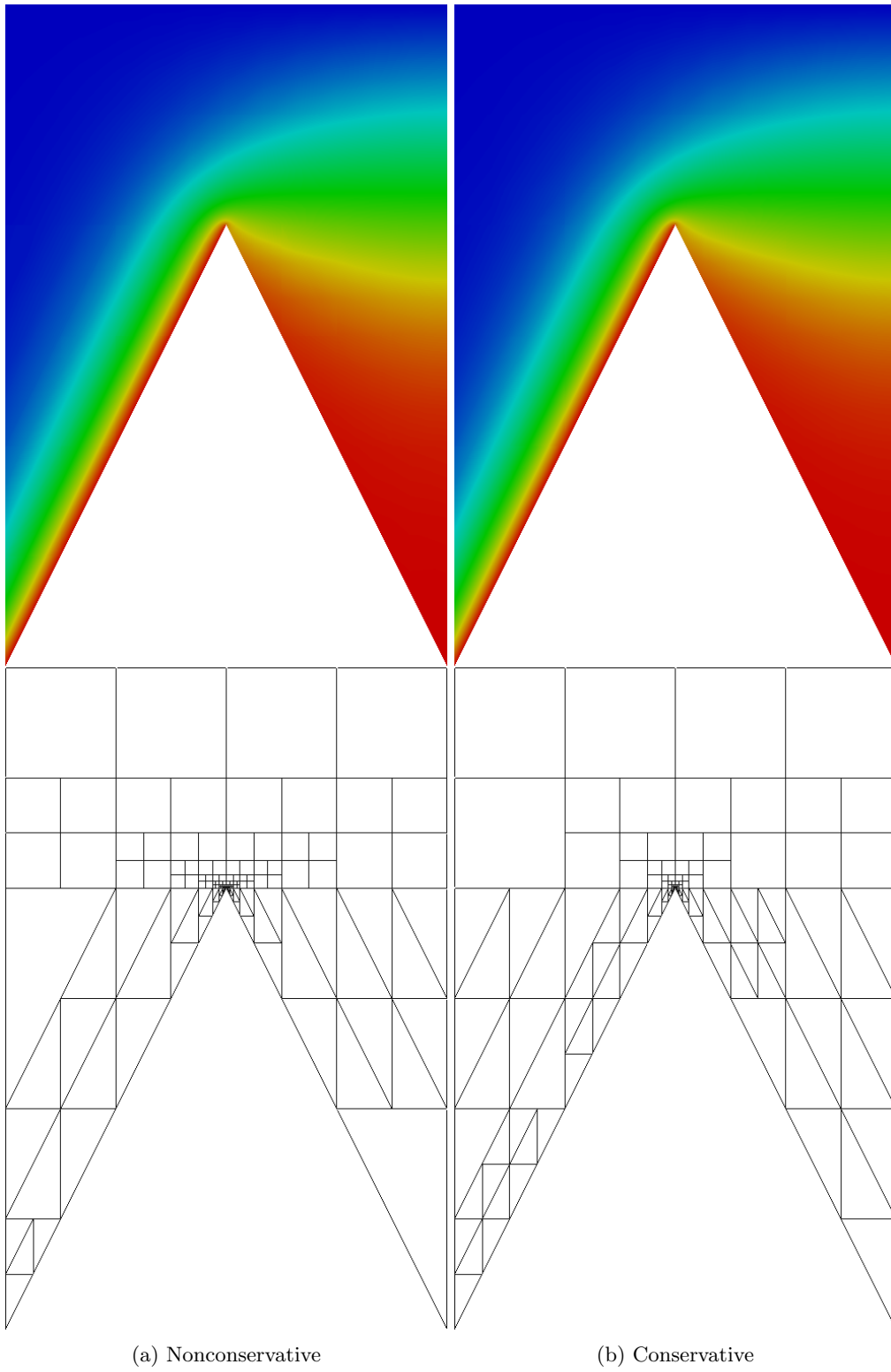


Figure 18: Wedge problem after 16 refinements

plots for the Erickson-Johnson problem, the energy levels for the two methods lie nearly right on top of each other. This seems to indicate at the least that enforcing local conservation doesn't hurt DPG too much.

Another measure of solution quality is to look at the magnitude of overshoots and undershoots in the solution. In most of the problems considered (barring the discontinuous source problem) the exact solution would range exactly between 0 and 1. The the resolved solutions, the divergence from these values would be negligible, but for the inner layer, in which $\epsilon = 10^{-6}$, we get overshoots and undershoots along the separation line. For the nonconservative formulation, the solution range for u was $[-0.392, 1.342]$, while the conservative solution range was $[0.389, 1.378]$. This difference is easily accounted for by the differences in refinement patterns between the two methods.

It is clear when comparing the refinement patterns that the two methods appear to calculate slightly different error representation functions (which determine which elements to adaptively refine). Standard DPG minimizes the error in the energy norm, but the Lagrange multipliers in the conservative formulation shift the solution slightly. So we should see somewhat higher error and different elements will get chosen for refinement. The choice of test norm also plays into this calculation of the error representation function. As discussed earlier, the conservative formulation allows us to throw away the L^2 term on v . The inclusion of this term required certain assumptions on β [3] that break down for the vortex problem. Here we see the nonconservative method needlessly refine in the center of the domain where the solution is constant. The conservative scheme is more discerning about refinements and focuses refinements where solution features are changing. In general, though, both methods appear to follow very similar refinement patterns.

It shouldn't come as a surprise that the conservative and nonconservative solutions match each other so closely. The conservative formulation enforces local conservation more strictly, but if we examine the flux imbalance plots, the nonconservative formulation is nearly conservative on its own – and appears to become more conservative with refinement. The flux imbalance of the conservative methods appears to bounce around close to the machine epsilon (plus a few orders of magnitude). The level of enforcement appears to creep up with more degrees of freedom, indicating possible accrument of numerical error.

References

- [1] J. Bramwell, L. Demkowicz, J. Gopalakrishnan, and W. Qiu. A locking-free hp DPG method for linear elasticity with symmetric stresses. *Num. Math.*, 2012. accepted.
- [2] J. Chan, L. Demkowicz, R. Moser, and N. Roberts. A class of Discontinuous Petrov–Galerkin methods. Part V: Solution of 1D Burgers and Navier–Stokes equations. Technical Report 25, ICES, 2010. submitted to J. Comp. Phys.
- [3] J. Chan, N. Heuer, T Bui-Thanh, and L. Demkowicz. Robust DPG method for convection-dominated diffusion problems ii: a natural inflow condition. Technical Report 21, ICES, 2012.
- [4] C. L. Chang and John J. Nelson. Least-squares finite element method for the stokes problem with zero residual of mass conservation. *SIAM J. Num. Anal.*, 34:480–489, 1997.
- [5] L. Demkowicz and J. Gopalakrishnan. A class of discontinuous Petrov-Galerkin methods. Part I: The transport equation. *Comput. Methods Appl. Mech. Engrg.*, 2009. accepted, see also ICES Report 2009-12.
- [6] L. Demkowicz and J. Gopalakrishnan. A class of discontinuous Petrov-Galerkin methods. Part II: Optimal test functions. *Numer. Meth. Part. D. E.*, 2010. in print.
- [7] L. Demkowicz and J. Gopalakrishnan. Analysis of the DPG method for the Poisson problem. *SIAM J. Num. Anal.*, 49(5):1788–1809, 2011.
- [8] L. Demkowicz and J. Gopalakrishnan. An overview of the DPG method. Technical report, ICES, 2013.
- [9] L. Demkowicz, J. Gopalakrishnan, I. Muga, and J. Zitelli. Wavenumber explicit analysis for a DPG method for the multidimensional Helmholtz equation. *Comput. Methods Appl. Mech. Engrg.*, 213-216:126–138, 2012.

- [10] L. Demkowicz, J. Gopalakrishnan, and A. Niemi. A class of discontinuous Petrov-Galerkin methods. Part III: Adaptivity. Technical Report 1, ICES, 2010. submitted to App. Num. Math.
- [11] L. Demkowicz and N. Heuer. Robust DPG method for convection-dominated diffusion problems. Technical Report 33, ICES, 2011.
- [12] J. F. Gerbeau, C. Le Bris, and M Bercovier. Spurious velocities in the steady flow of an incompressible fluid subjected to external forces. *International Journal for Numerical Methods in Fluids*, 25(6):679–695, 1997.
- [13] D. Griffiths. The ‘no boundary condition’ outflow boundary condition. *International Journal for Numerical Methods in Fluids*, 24(4):393–411, 1997.
- [14] D. Moro, N.C. Nguyen, and J. Peraire. A hybridized discontinuous Petrov-Galerkin scheme for scalar conservation laws. *Int.J. Num. Meth. Eng.*, 2011. in print.
- [15] J. B. Perot. Discrete conservation properties of unstructured mesh schemes. *Annual Review of Fluid Mechanics*, 43:299–318, 2011.
- [16] Nathan V. Roberts, Tan Bui-Thanh, and Leszek F. Demkowicz. The DPG method for the Stokes problem. Technical Report 12-22, ICES, 2012.
- [17] H. Roos, M. Stynes, and L. Tobiska. *Robust numerical methods for singularly perturbed differential equations: convection-diffusion-reaction and flow problems*. Springer series in computational mathematics. Springer, 2008.

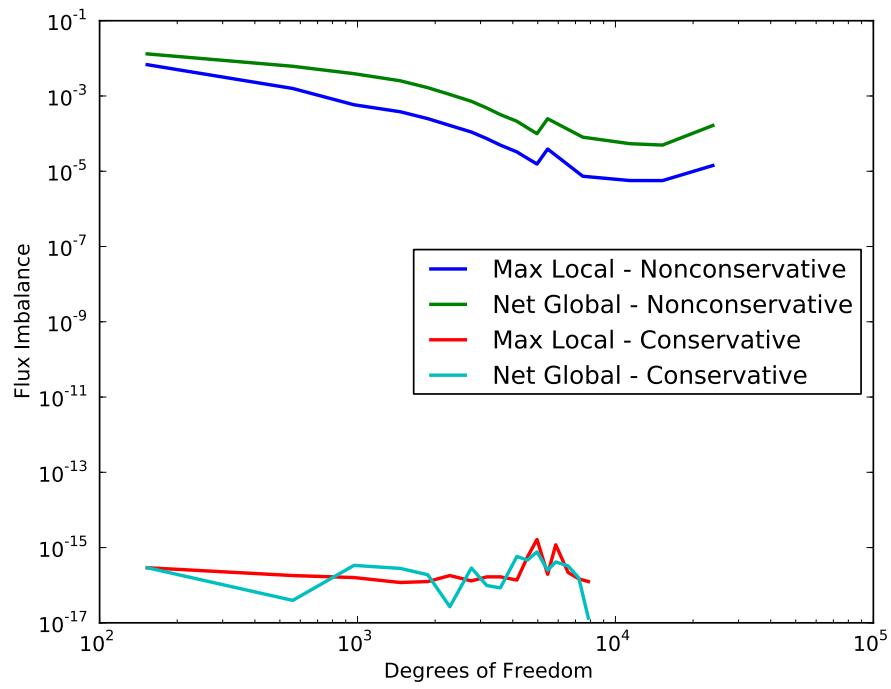


Figure 19: Flux imbalance in wedge solutions

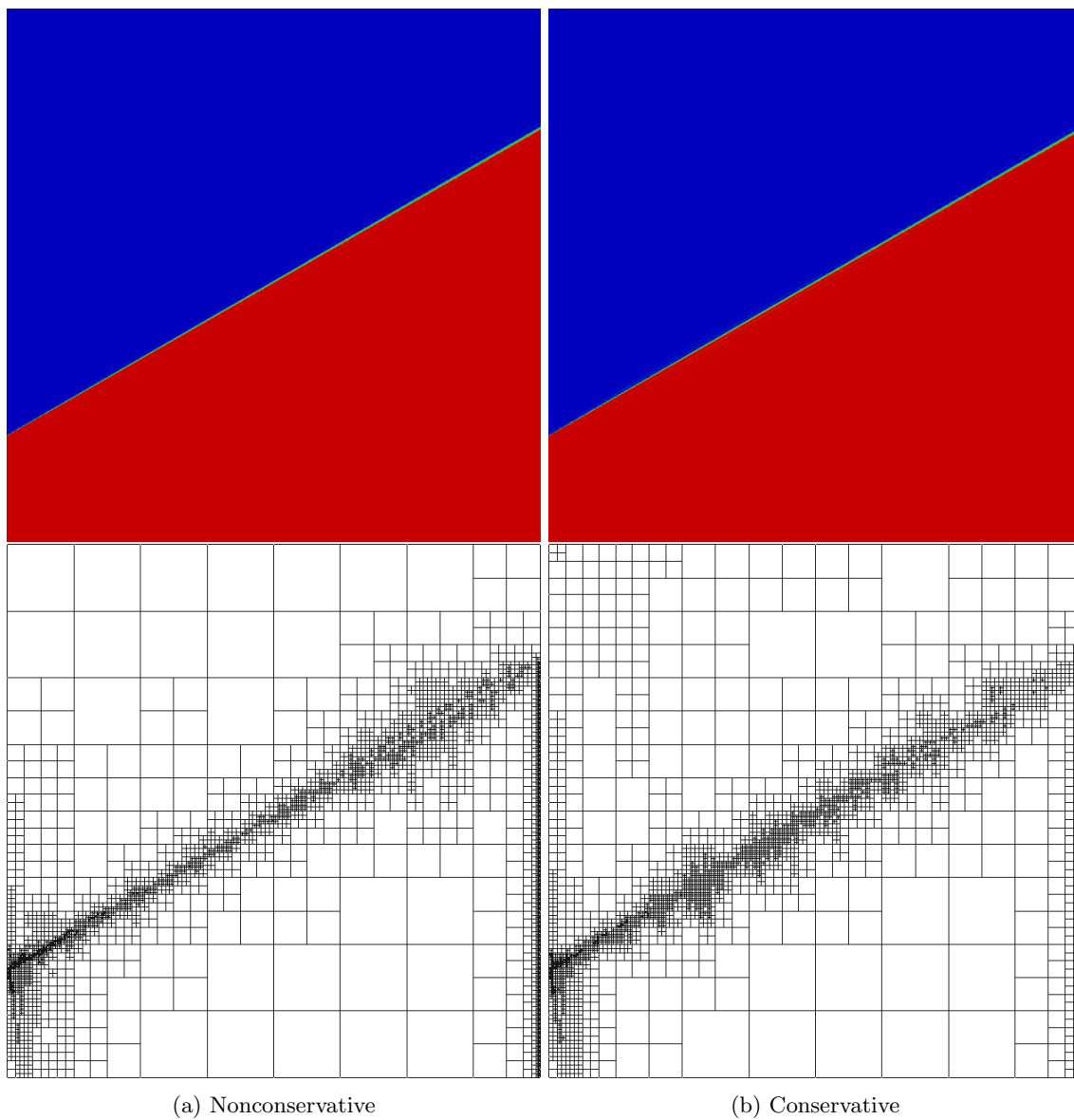


Figure 20: Inner layer problem after 8 refinements

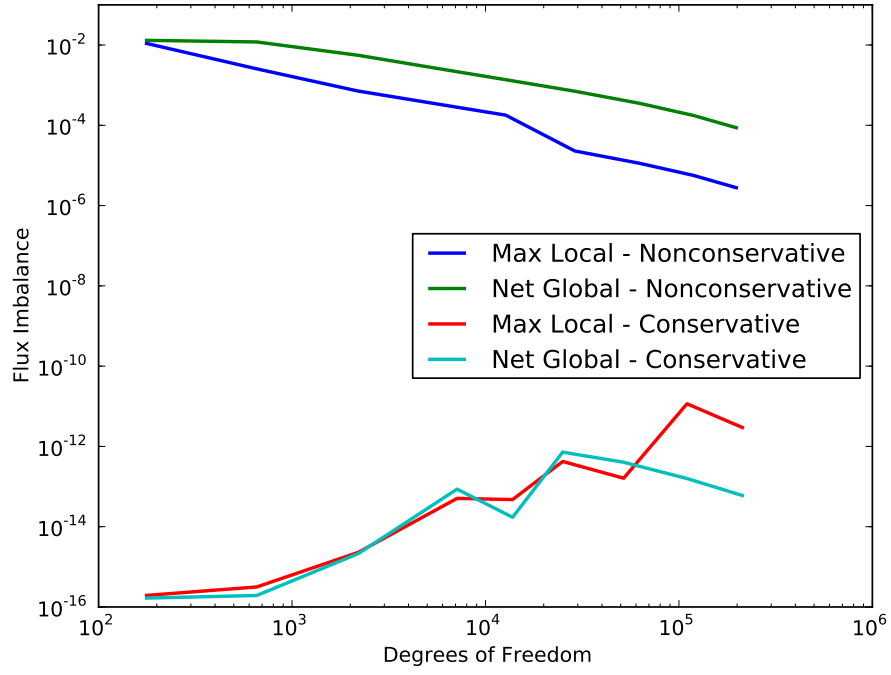


Figure 21: Flux imbalance in inner layer solutions

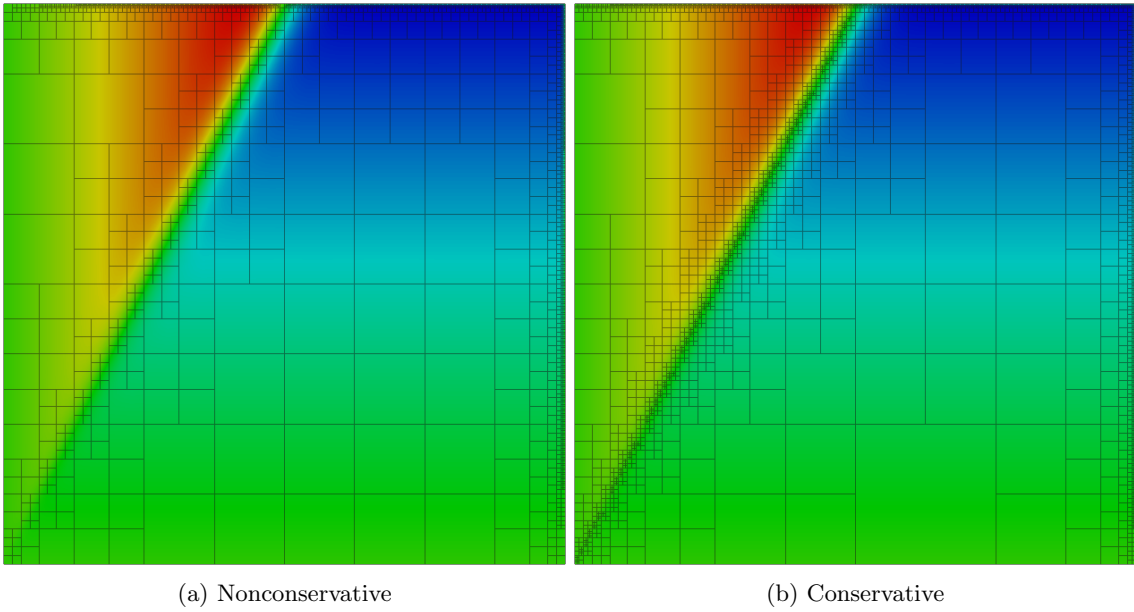


Figure 22: Discontinuous source problem after 8 refinements

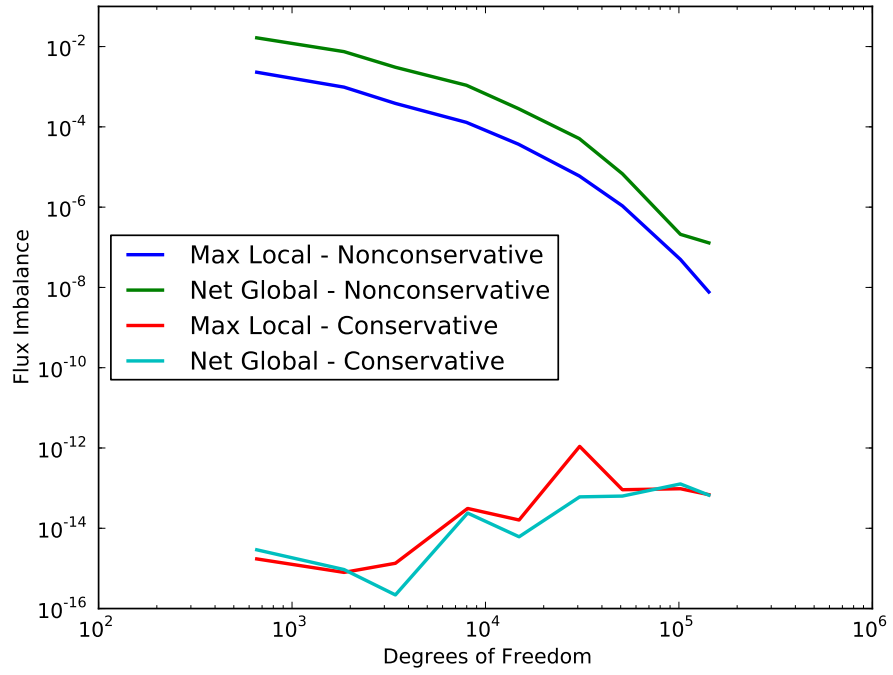


Figure 23: Flux imbalance in discontinuous source solutions

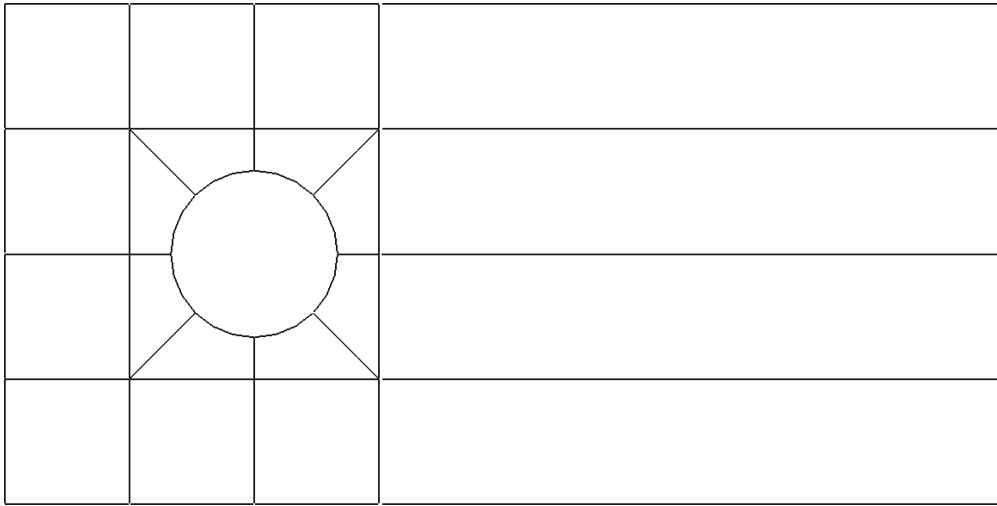
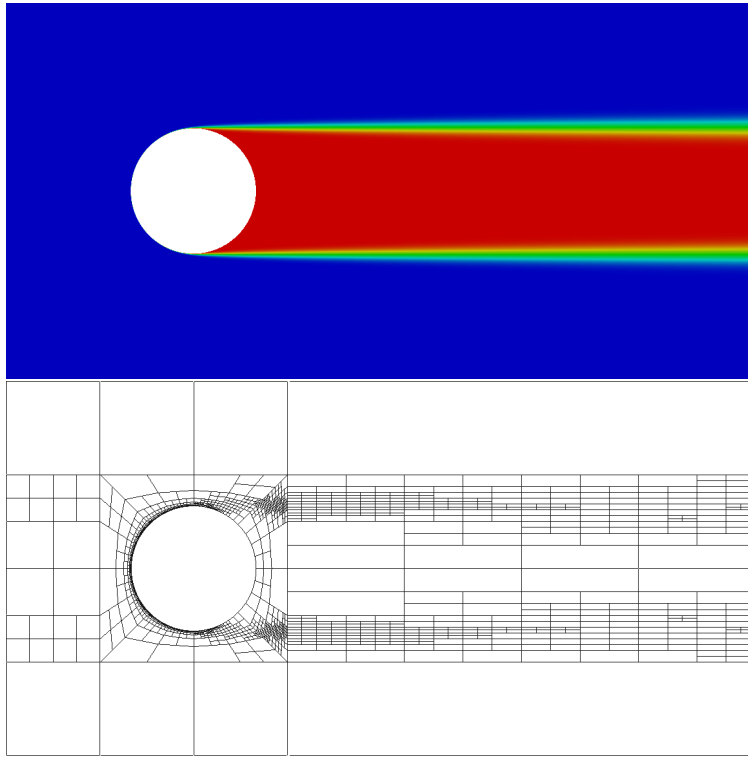
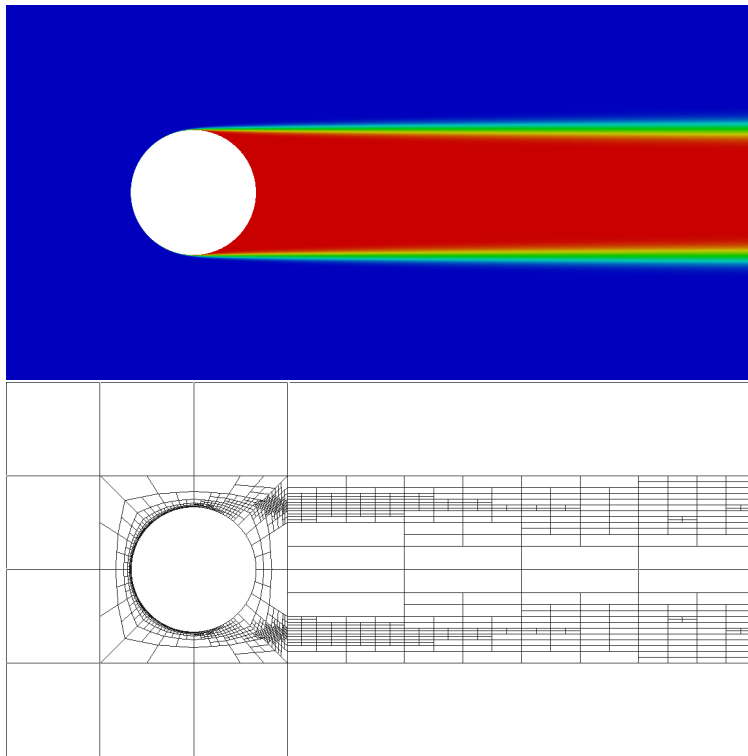


Figure 24: Initial mesh for the Hemker problem



(a) Nonconservative



(b) Conservative

Figure 25: Hemker problem after 8 refinements

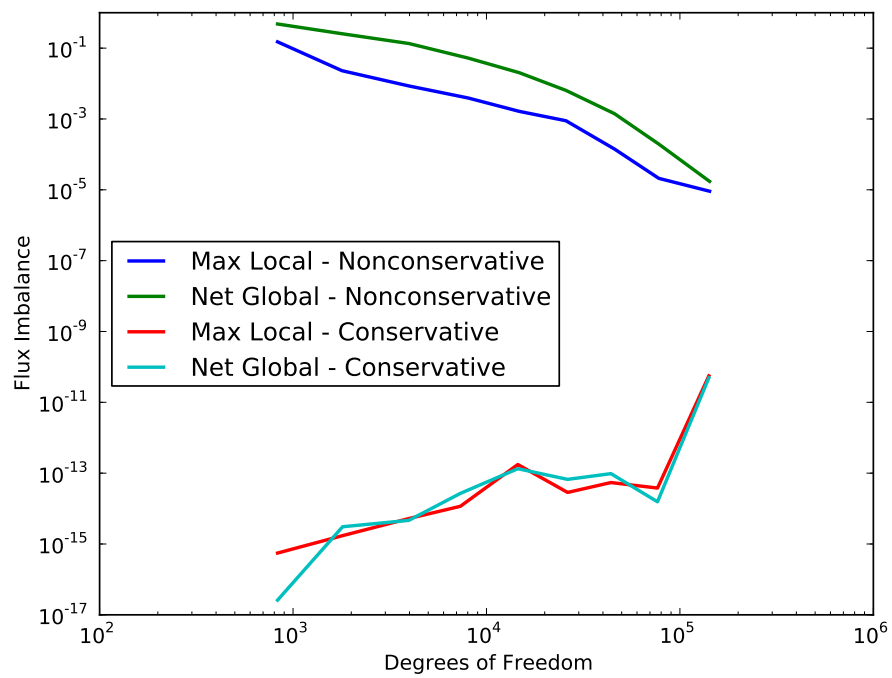


Figure 26: Flux imbalance in Hemker problem